GA–A27418

THE ROLE OF ZONAL FLOWS AND PREDATOR-PREY OSCILLATIONS IN THE FORMATION OF CORE AND EDGE TRANSPORT BARRIERS

by
L. SCHMITZ, L. ZENG, T.L. RHODES, J.C. HILLESHEIM,
W.A. PEEBLES, R.J. GROEBNER, K.H. BURRELL, G.R. McKEE,
Z. YAN, G.R. TYNAN, P.H. DIAMOND, J.A. BOEDO,
E.J. DOYLE, B.A. GRIERSON, C. CHRYSTAL,
M.E. AUSTIN, W.M. SOLOMON and G. WANG

OCTOBER 2012

GENERAL ATOMICS

DISCLAIMER

GA–A27418

THE ROLE OF ZONAL FLOWS AND PREDATOR-PREY OSCILLATIONS IN THE FORMATION OF CORE AND EDGE TRANSPORT BARRIERS

by
L. SCHMITZ,[1] L. ZENG,[1] T.L. RHODES,[1] J.C. HILLESHEIM,[1]
W.A. PEEBLES,[1] R.J. GROEBNER, K.H. BURRELL, G.R. McKEE,[2]
Z. YAN,[2] G.R. TYNAN,[3] P.H. DIAMOND,[3] J.A. BOEDO,[3]
E.J. DOYLE,[1] B.A. GRIERSON,[4] C. CHRYSTAL,[3]
M.E. AUSTIN,[5] W.M. SOLOMON[4] and G. WANG[1]

This is a preprint of a paper to be presented at the 24th IAEA Fusion Energy Conference, October 8–13, 2012 in San Diego, California and to be published in Proceedings.

[1]University of California-Los Angeles, Los Angeles, California USA
[2]University of Wisconsin-Madison, Madison, Wisconsin USA
[3]University of California San Diego, La Jolla, California USA
[4]Princeton Plasma Physics Laboratory, Princeton, New Jersey USA
[5]University of Texas-Austin, Austin, Texas USA

Work supported by
the U.S. Department of Energy
under DE-FG03-01ER54615, DE-FG02-08ER54984,
DE-FC02-04ER54698, DE-FG02-89ER53296,
DE-FG02-08ER54999, DE-AC02-09CH11466
and DE-FG02-07ER54917

GENERAL ATOMICS PROJECT 30200
OCTOBER 2012

ABSTRACT

We present direct evidence of low frequency Zonal Flows (ZF) initiating formation of an electron internal transport barrier (ITB) at the q=2 rational surface via local suppression of electron-scale turbulence. Zonal Flows are also observed to trigger the L- to H-mode transition via periodic turbulence suppression in limit-cycle oscillations (LCO) near the transition power threshold, consistent with predator-prey dynamics. The final transition to ELM-free H-mode occurs after the equilibrium $\boldsymbol{E}\times\boldsymbol{B}$ flow shear increases due to ion pressure profile evolution. Multi-channel Doppler Backscattering (DBS) has revealed the radial structure of the ZF-induced shear layer and the $\boldsymbol{E}\times\boldsymbol{B}$ shearing rate $\omega_{\boldsymbol{E}\times\boldsymbol{B}}$ in both barrier types. The time-dependent flow shear and the turbulence envelope are anti-correlated (180º out of phase) in the ITB. During edge barrier formation, the shearing rate lags the turbulence envelope during the LCO by 90º, transitioning to anti-correlation (180º) as the equilibrium shear due to the increasing edge pressure gradient becomes dominant. LCO with time-reversed evolution dynamics (transitioning from an equilibrium-flow dominated to a ZF-dominated state) have also been observed during the H-L back-transition and are potentially of interest for controlled ramp-down of β_θ in ITER.

1. INTRODUCTION

Understanding the physics and formation dynamics of core and edge transport barriers is of crucial importance for extrapolating present tokamak performance to burning plasma regimes. Internal transport barriers (ITBs) can form spontaneously with sufficient auxiliary or α-particle heating and directly affect core temperature and thermal confinement, as well as the ratio of electron-to-ion temperature and fusion yield. Accurate modeling of the L-H power threshold beyond the present empirical scaling laws is required for future burning plasma experiments, taking into account plasma shaping, divertor geometry, the beam-induced and intrinsic torque, and collisionality. It has been recognized early that $\boldsymbol{E}\times\boldsymbol{B}$ flow shear maintains turbulence suppression in the H-mode pedestal as well as in internal barriers [1–4]. With neutral beam injection and driven ion rotation v_i, barriers can be supported via sheared $\boldsymbol{E}\times\boldsymbol{B}$ rotation resulting from the v_ixB term in the radial momentum balance, or due to the ion pressure gradient, depending on the plasma regime, barrier evolution, and other experimental details [5–7]. The trigger initiating turbulence suppression and barrier formation has not been conclusively identified for either core or edge barriers, although recent experimental evidence [8–14] and theoretical modeling [15,16] point strongly towards turbulence-generated $\boldsymbol{E}\times\boldsymbol{B}$ flows (or Zonal Flows) as the crucial element. The energy transfer from the turbulence spectrum into low frequency turbulence-driven flows, via the nonlinear Reynolds stress, has been directly measured recently, supporting this physical picture [17,18]. In this paper, we present evidence of radially localized low frequency Zonal Flows suppressing electron-scale turbulence ($k_\theta\rho_s$~2) and initiating formation of an electron ITB at the q=2 rational surface (Section 2). Section 3 discusses low frequency limit cycle oscillations triggering turbulence suppression in the wavenumber range consistent with Ion Temperature Gradient (ITG) modes and/or Resistive Ballooning Modes (RBM), and initiating the L- to H-mode transition near the power threshold. For heating power well above threshold, rapid transitions executing only a partial limit cycle are observed. In both cases, increasing equilibrium shear locks in the final transition to H-mode confinement as the ion pressure gradient increases (either gradually or fast) due to (locally) reduced radial particle and heat flux. Limit cycle oscillations during the H-L back-transition are discussed in Section 4. Finally, a summary and comparison of the observed Zonal Flow characteristics and trigger dynamics in edge and core transport barriers is given in Section 5.

2. ZONAL FLOWS TRIGGERING ELECTRON ITB FORMATION

With early neutral beam heating in DIII-D during current ramp, ion and electron internal transport barriers are routinely formed as the safety factor reduces and successive rational q-surfaces enter the plasma [8,19,20]. Earlier work on DIII-D has detailed how ITBs in reversed shear L-mode plasmas are triggered when the q=2 surface enters the plasma [8,19]. Earlier theoretical work has ascribed the trigger to the rarefaction of rational magnetic surfaces around q=2, giving rise to local zero-mean frequency Zonal Flow structures [20]. Indications of transient, localized $\boldsymbol{E}\times\boldsymbol{B}$ flows during ion ITB formation have been previously observed by Beam Emission Spectroscopy (BES). Here we report simultaneous measurements of $\boldsymbol{E}\times\boldsymbol{B}$ velocity and electron-scale density fluctuation amplitude during electron ITB formation. These measurements employ multi-channel microwave Doppler Backscattering (DBS). Doppler Backscattering [21,22] on DIII-D utilizes multi-frequency, co-linear diagnostic microwave beams launched at an oblique angle to the magnetic flux surfaces. Backscattering by plasma density fluctuations occurs preferentially near the cutoff layer [21], according to the selection rules $k_s = -k_I = 2k_\theta$ and $\omega_s = \omega_I + v_t k_\theta$, where the indices I and s denote the incident and backscattered wave, v_t is the poloidal turbulence advection velocity, and k_θ is the resonant poloidal density fluctuation wavenumber. The backscattered signal amplitude is proportional to the density fluctuation amplitude $\tilde{n}(k_\theta)$. The probed wavenumber k_θ, and the probed major radius R are obtained using ray tracing. The time-resolved $\boldsymbol{E}\times\boldsymbol{B}$ velocity is obtained from the instantaneous Doppler shift, $f_d = (\omega_R - \omega_I)/2\pi = v_\perp k_\theta/(2\pi)$, with $v_\perp = v_{\boldsymbol{E}\times\boldsymbol{B}} + v_{ph}$ [23]. Neglecting the (typically small) contribution of the fluctuation phase velocity v_{ph}, one obtains $v_{\boldsymbol{E}\times\boldsymbol{B}} \approx 2\pi f_D/k_\theta$.

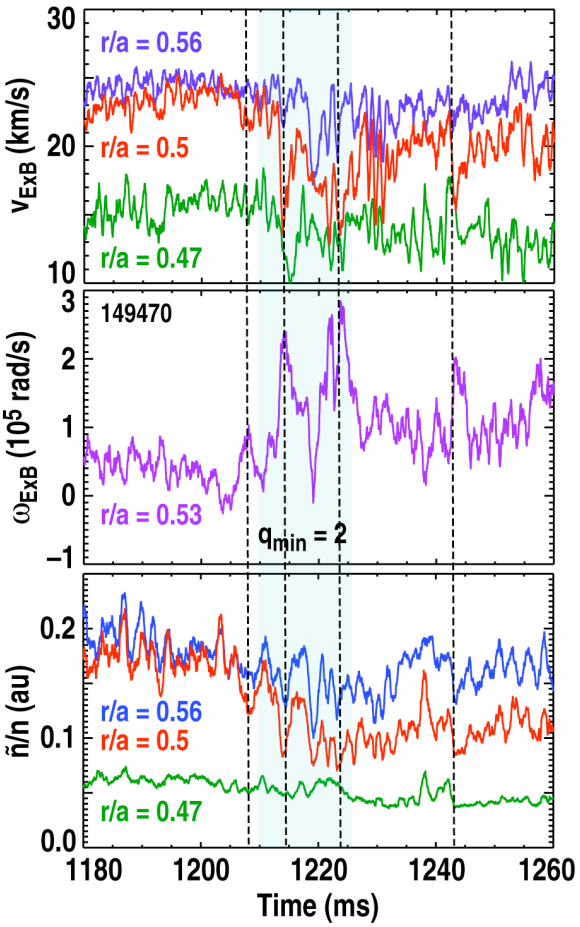

FIG. 1. Time evolution of (a) $\boldsymbol{E}\times\boldsymbol{B}$ velocity; (b) shearing rate at r/a=0.5 during electron ITB formation; (c) normalized density fluctuation amplitude near the q=2 surface.

Figure 1 shows the time evolution of the $\boldsymbol{E}\times\boldsymbol{B}$ flow velocity, the $\boldsymbol{E}\times\boldsymbol{B}$ flow shear (determined from the difference in flow velocity between neighboring DBS channels), and the density fluctuation amplitude at three radii as an electron ITB is formed near r/a=0.5 during plasma current ramp in a reversed-shear L-mode plasma (line

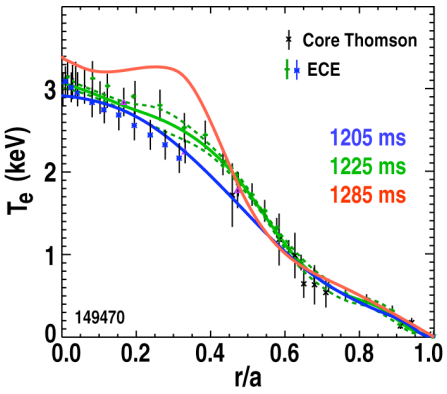

FIG. 2. Radial electron temperature profile at 1205–1285 ms, indicating electron ITB formation at r/a ~0.5.

averaged density $\langle n \rangle = 2.1 \times 10^{13}$ cm^{-3}, $B_\phi = 2$T). The probed poloidal wavenumber is $k_\theta \rho_s \sim 2$ (with a wavenumber resolution $\Delta k_\theta / k_\theta \sim 0.5$). Motional Stark Effect Polarimetry (MSE) indicates that $q_{\min} = 2$ enters the plasma at 1210–1220 ms, at a radius $r/a \sim 0.5 \pm 0.05$. The shearing rate for $r/a \sim 0.5$ increases within ~200 μs at $t \sim 1212$ ms, and fine-scale radial structure in the $\boldsymbol{E}\times\boldsymbol{B}$ flow begins to evolve near $r/a \sim 0.5$ [Fig. 1(c)], starting at $t \sim 1207$ ms, as the $q=2$ surface enters the plasma. We attribute this drop in $v_{\boldsymbol{E}\times\boldsymbol{B}}$ and the resulting radial flow shear to local Zonal Flow excitation from the turbulence spectrum in the vicinity of the $q=2$ surface. Stepwise reductions in the electron-scale density fluctuation level are observed in the two outer DBS chords spanning $0.5 \le r/a \le 0.56$, for 1207 ms $< t <$ 1224 ms, concomitantly with large increases in local shear as indicated by dashed vertical lines, and a sustained decrease in fluctuation level is obvious in particular for $r/a = 0.5$.

The time evolution of the radial electron temperature profile, measured via both Electron Cyclotron Emission and Thomson Scattering, is shown in Fig. 2. Local steepening of the electron temperature gradient is evident at 1225 ms (about 10 ms after the ITB trigger event), with the electron ITB fully developed after 1270 ms (shown here is data for 1285 ms). The $q=2$ surface splits eventually as $q_{\min}$ reduces further after 1240 ms and a concomitant ion ITB forms after 1260 ms inboard of $r/a = 0.4$ (inside the minimum radius that DBS can probe at this density, and not shown here).

A detailed measurement of a quasi-stationary shear layer has been made in a different shot (133678), where an electron ITB has been maintained for several hundred ms, and the position of the $q=2$ surface was relatively constant (Fig. 3). A DBS system with four closely spaced channels has been used (with channel separation $\Delta r_{ch} \sim 0.5$ cm, as determined by the experimental electron density gradient). A fine-scale, radial double shear layer with positive outboard and negative inboard $\boldsymbol{E}\times\boldsymbol{B}$ flow shear [$\Delta r \sim 4$–$6\rho_s \sim 1.5$–2 cm, Fig. 3(b)] is observed at the $q=2$ surface. The level of

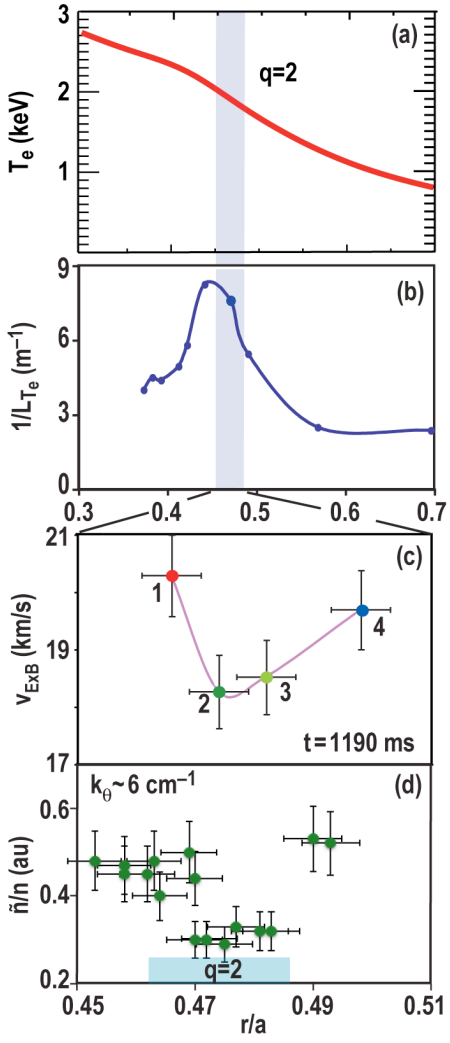

FIG. 3. Radial profiles of (a) electron temperature; (b) inverse temperature gradient scale length; (c) $\boldsymbol{E}\times\boldsymbol{B}$ velocity, and (d) normalized density fluctuation level ($k_\theta \rho_s \sim 2$), across the electron transport barrier.

electron-scale density fluctuations ($k_\theta \rho_s \sim 2$) is reduced in the region of sheared flow [Fig. 3(c)]. In contrast to earlier observations of turbulence suppression in an ion ITBs near q=2 [8], no large-scale barrier is obvious here in the ion temperature (or density) profile, but the CER/Thomson scattering diagnostic chords are too coarsely spaced to detect possible localized steepening of the ion temperature/pressure profile which may sustain the electric field well once turbulence and ZF decay during barrier formation. The $\boldsymbol{E}\times\boldsymbol{B}$ flow is composed of steady-state and broadband components (with a frequency spectrum $f_d \leq$ 5 kHz). Anti-correlation of shear and density fluctuation amplitude (Fig. 4) is found in the inboard and outboard shear layer, with an embedded shear-free zone [Fig. 4(b)].

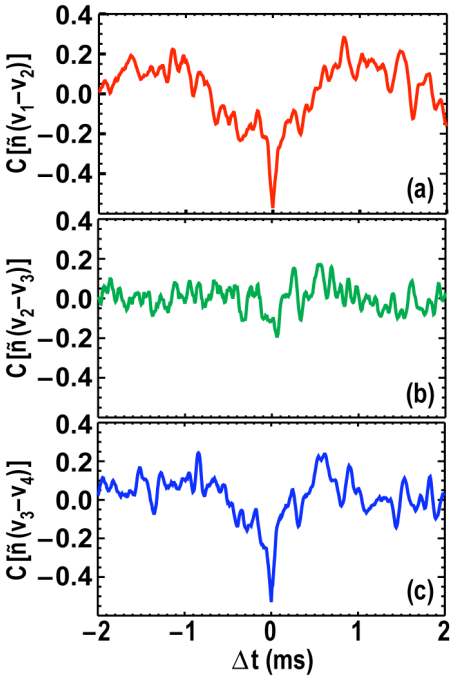

FIG. 4. Cross correlation coefficient between rms density fluctuation level and $\boldsymbol{E}\times\boldsymbol{B}$ flow shearing rate; velocity indices correspond to measurement locations shown in Fig. 3(c); (a) ch 1-2; (b) ch 2-3; (c) ch 3-4.

3. PREDATOR-PREY LIMIT CYCLE TRIGGERING THE L-H TRANSITION

Evidence of turbulence-generated shear flows preceding the L-H transition has been recently observed in several experiments [8–14]. In DIII-D, near the LH-transition power threshold (~4 MW neutral beam co-injection into an L-mode plasma with line-averaged density $\langle n \rangle$~2.5x 10^{13} cm^{-3}, $B_\phi = 2$ T, and plasma current $I_p = 1.1$ MA), extended LCO between the $\boldsymbol{E}\times\boldsymbol{B}$ velocity and the density fluctuation envelope $\tilde{n}$, inside the last closed flux surface (LCFS) [14] have been clearly observed to trigger edge barrier formation and periodically reduce local transport leading up to the H-mode transition. Figure 5(a) shows a time evolution contour plot of the $\boldsymbol{E}\times\boldsymbol{B}$ velocity across and inside the last closed flux surface (LCFS), determined via multi-channel DBS from turbulence poloidal advection [22,23]. Twelve radial locations are probed simultaneously using co-linear launch/receive optics. The DBS probing locations (X-mode cut-off layer) were determined for this data set based on high time resolution (25 μs) electron density profiles from profile reflectometry. When the LCO starts at 1271.7 ms, the $\boldsymbol{E}\times\boldsymbol{B}$ velocity periodically becomes negative at and just inside the last closed flux surface (LCFS). The negative flow increases with time and the flow layer expands radially. Around 1288 ms, the transition to ELM-free H-mode takes place after a final transient, characterized by a wider, steady flow layer. Figure 5(b) shows

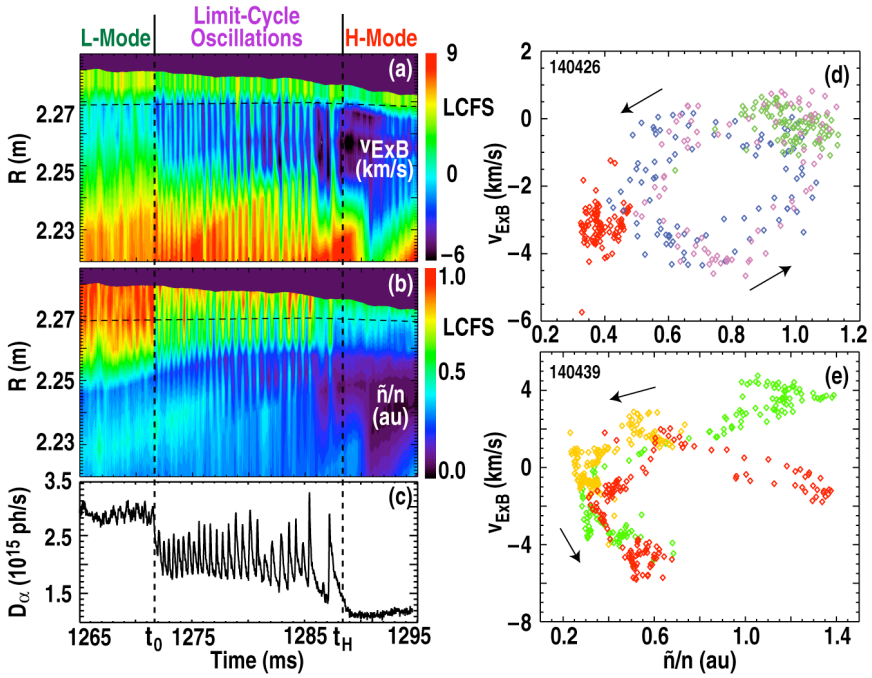

FIG. 5. (a) $\boldsymbol{E}\times\boldsymbol{B}$ velocity, (b) normalized density fluctuation level ñ/n, and (c) D_α signal. (d) Limit cycle between density fluctuation level and $v_{\boldsymbol{E}\times\boldsymbol{B}}$ during the LCO, the start of the LCO (t_0) and the final transition to H-mode (t_H) are indicated; (e) partial limit cycle during the "regular" L-H transition; 0.5 cm inside the LCFS (green); 1.8 cm inside the LCFS (red); and 4 cm inside the LCFS (orange).

that the normalized density fluctuation level $\tilde{n}/n$ (proportional to the amplitude of the scattered DBS signal) is periodically reduced during the LCO (the probed poloidal wavenumber is $k_\theta\rho_s$~0.45 with $\Delta k_\theta/k_\theta$~ 0.3, encompassing the most unstable ITG and RBM wavenumber range). Sustained turbulence reduction is observed at the H-mode transition at t_H ~1288 ms [Fig. 5(b)]. The periodic decrease in the D_α recycling light indicates modulation of the radial particle outflux past the LCFS [Fig. 5(c)] due to periodically improved radial particle confinement.

The limit cycle between $\tilde{n}/n$ and $v_{\boldsymbol{E}\times\boldsymbol{B}}$ is shown in Fig. 5(d). $\boldsymbol{E}\times\boldsymbol{B}$ flow oscillations lag $\tilde{n}/n$ by 90º (magenta/ purple data points taken during a 3 ms time interval starting at t=1278 ms during the LCO, 1 cm and 2.5 cm inside the LCFS; green symbols correspond to L-mode, red symbols to H-mode). The limit cycle dynamics reflects a predator-prey relationship between the $\boldsymbol{E}\times\boldsymbol{B}$ flow generated from the turbulence via the nonlinear Reynolds stress, and the energy density in the turbulence. As the turbulence level grows with increasing neutral beam heating power in L-mode, ZFs are eventually triggered at and just inside the separatrix where the fluctuation level and energy density are highest. The flow shear associated with the ZF reduces the turbulence saturation level. In turn the ZF cannot be sustained due to the decreasing turbulence level. Once the ZF shear is too small to maintain turbulence reduction the turbulence level grows again to the point where ZFs are triggered, and the cycle repeats.

We have shown in [14] that the LCO has all characteristics of a Zonal Flow predator-prey oscillation characterized by toroidal/poloidal symmetry (n=0, m=0), a finite radial wavenumber (k_r~0.7 cm^{-1} at t=1275 ms), and a 90º phase lag of the ZF with respect to the density fluctuation envelope $\tilde{n}/n$.

In a "regular" L-H transition in the same lower single null divertor configuration (140439), but with beam power above threshold (L-mode density $\langle n\rangle$ ~ 1.5x10^{19} cm^{-3}), turbulence-driven, toroidally and poloidally symmetric flows (n,m=0) have been documented as short transients executing only part of one limit cycle period over ~1.5 ms [Fig. 5(e), showing three data sets for major radii 0.5–4 cm inside the LCFS]. Figure 6 shows the corresponding time evolution of density fluctuations [Fig. 6(a,c)], the total $\boldsymbol{E}\times\boldsymbol{B}$ shearing rate $\omega_{\boldsymbol{E}\times\boldsymbol{B}}$ and turbulence decorrelation rate $\Delta\omega_D$ [Fig. 6(b,d)], and the radial density gradient [Fig. 6(e)]. Just inside the LCFS, the density fluctuation level decreases as the flow shearing rate

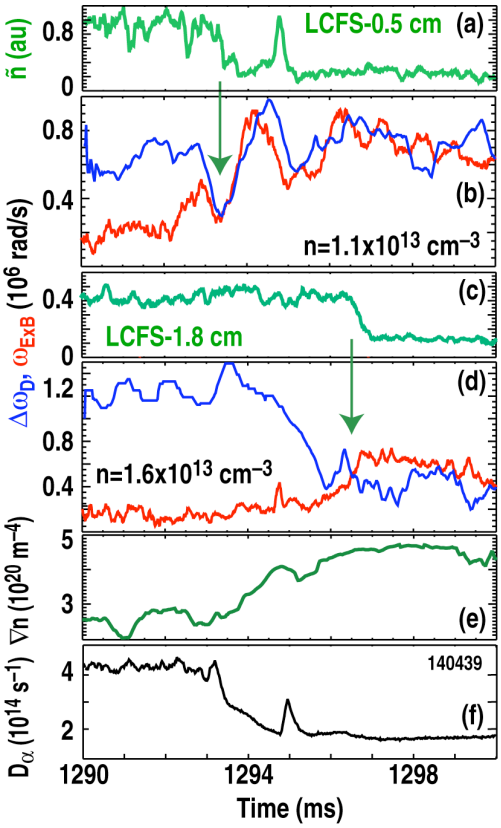

FIG. 6. (a) Density fluctuation level; (b) decorrelation and shearing rates 0.5 cm inside the LCFS; (c) density fluctuation level; (d) decorrelation and shearing rates 1.8 cm inside the LCFS; (e) density gradient spanning the two radii; (f) D_α signal.

exceeds the decorrelation rate [Fig. 6(a,b)]. A brief flow oscillation corresponding to a partial LCO cycle [Fig. 5(e)] is evident. Radial transport begins to decrease as reflected in the D_α signal [Fig. 6(f)]. Further inboard, the decorrelation rate decreases slowly, and the flow shearing rate increases with a delay of several milliseconds compared to the outboard location, again suppressing fluctuations once $\omega_{E\times B} > \Delta\omega_D$. The increase in $\omega_{E\times B}$ is in part due to the increasing diamagnetic flow contribution, as the density (pressure) gradient steepens after the initial fluctuation suppression near the LCFS.

Hence the "regular" transition exhibits a similar phenomenology, on a condensed time scale, as the extended LCO transition. Turbulence suppression due to ZF shearing is first observed in both transition types near the separatrix when the turbulence decorrelation rate $\Delta\omega_D$ decreases sharply concomitantly with an increasing $\boldsymbol{E}\times\boldsymbol{B}$ shearing rate $\omega_{E\times B}$ due to ZF onset.

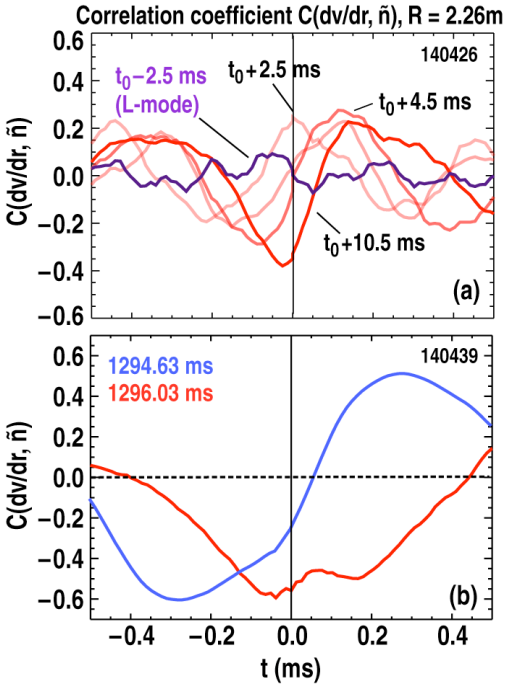

FIG. 7. Cross-correlation coefficient between the $\boldsymbol{E}\times\boldsymbol{B}$ shearing rate and the density fluctuation level; (a) for different times with respect to the start time t_0 of the LCO; (b) in the "regular" transition during the abbreviated limit cycle (1294.63 ms) and at 1296.03 ms just before the final D_α drop (indicating completion of H-mode transition).

We have previously shown that equilibrium shear due to the gradually increasing ion pressure gradient becomes important later during the LCO (1280–1286 ms) [14]. At these times the equilibrium shear due to the diamagnetic contribution to E_r becomes dominant after the ZF decays during the predator-prey cycle, delaying the recovery of the turbulence after the ZF has collapsed. This increased delay slows down the limit cycle frequency, as seen in Fig. 1. This observation is consistent with the two-predator, one prey model advanced presently [19,20], where the ZF (predator 1) is eventually eclipsed by the equilibrium flow shear (predator 2). Strong experimental evidence for the two-predator, one-prey concept comes from the time evolution of the phase shift between $\tilde{n}/n$ and the shearing rate $\omega_{E\times B}$ (Fig. 7). Early during the LCO, $v_{E\times B}$ lags $\tilde{n}/n$ by roughly 90°, consistent with a predator-prey cycle between $\tilde{n}/n$ and $\omega_{E\times B}$. Later during the LCO, just before steady (ELM-free) H-mode confinement is realized, the phase shift increases to 180° in both the extended LCO and the regular transition (Fig. 7). A phase shift near 180° represents a strong indication that equilibrium shear is dominating the oscillatory ZF shear.

4. LIMIT CYCLE OSCILLATIONS DURING THE H-L BACK-TRANSITION

Limit cycle oscillations were also recently observed during the H-L back-transition (Fig. 8), showing similar predator-prey characteristics and behavior complementary to the forward transition. The H-L back transition and in particular the H-LCO-L back transition sequence are important to investigate the interaction between core and edge turbulence and turbulence spreading [24]. Figure 8 shows first an H-LCO back transition where the ZF frequency [Fig. 8(c)] increases with time (reflecting a diminishing influence of the equilibrium shear) and the ZF amplitude decreases with time, eventually leading to the LCO-L back-transition. Well into the LCO period $\omega_{E\times B}$ lags $\tilde{n}/n$ by 90º as seen in the forward transition discussed earlier. Hence the forward transition sequence is reversed, while the 90º phase lag of $\omega_{E\times B}$ with respect to $\tilde{n}$ is preserved. Around 3610 ms, a forward L-LCO transition occurs, about 100 ms after the neutral beam power has been increased, with the limit cycle frequency showing the characteristic slow-down, then transitioning to steady ELM-free H-mode around 3960 ms. There is a clear hysteresis in onset neutral beam heating power at the H-LCO back-transition and the LCO-L back-transitions compared to the respective forward transitions.

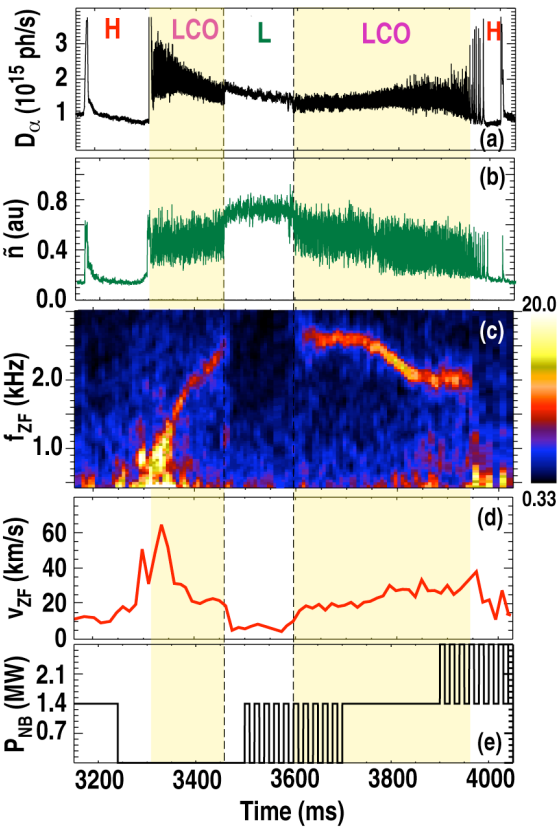

FIG. 8. (a) D_α recycling light, (b) ñ, (c) ZF (LCO) frequency; (d) magnitude of $\boldsymbol{E}\times\boldsymbol{B}$ velocity, and (e) neutral beam power during H-L and L-H transitions with LCO.

Back-transition LCOs are potentially important for controlled rampdown of β_θ in ITER, as they may assist in achieving a "soft landing" of the discharge without vertical displacement events. It should be noted that the H-LCO back-transition shown in Fig. 8 is initiated by a Type-I ELM event (visible in the D_α data) which may transiently reduce the equilibrium ion pressure gradient and related equilibrium shear, and thus allow the Zonal Flow to grow. Further research is in progress to identify under which conditions back-transition LCOs can be initiated without ELM trigger.

5. CONCLUSIONS

In this paper we have presented evidence that both core and edge transport barriers are triggered via transient low frequency turbulence-generated flows. A similar well structure in the radial electric field (and $\boldsymbol{E}\times\boldsymbol{B}$ velocity) forms in both barrier types, with radial extent ~ 4–6 ρ_s in the electron ITB and ~ 10–20 ρ_s in the edge barrier, although the radial ZF structure in the ITB can be more complex. Similarities between both barrier types include a region free of $\boldsymbol{E}\times\boldsymbol{B}$ shear embedded within an outer (positive) and inner (negative) shear layer. The ZF shear layer in the electron ITB forms during q-profile evolution as $q_{\min}$~2, roughly at plasma mid radius. Direct evidence for suppression of electron-scale density fluctuations has been found, with a 180º phase shift between fluctuation level and shearing rate. We conjecture that the equilibrium pressure gradient eventually increases locally, maintaining the $\boldsymbol{E}\times\boldsymbol{B}$ shear layer after fluctuations subside and the turbulence-driven ZF is damped. In contrast, near the L-H transition power threshold the edge barrier is triggered via extended predator-prey limit cycle oscillations, with an initial phase shift of 90º between $\tilde{n}$ and $\omega_{\boldsymbol{E}\times\boldsymbol{B}}$. Only later during the LCO this phase shift transitions to 180º as equilibrium shear from pressure profile evolution becomes dominant, eventually sustaining turbulence suppression in the transition to steady ELM-free H-mode. Abbreviated LCO cycles are observed in "regular" L-H transitions indicating a universal two-stage transition dynamics where transient turbulence-generated shear flow triggers the initial fluctuation suppression in a narrow layer at and just inside the separatrix, and equilibrium shear locks in the transition once the edge pressure gradient has locally increased. Limit cycle oscillations are also observed during the H-L back transition, with evolution dynamics reversed compared to the forward transition. In the initial data shown here, pedestal pressure profile relaxation due to a type-I ELM precedes the LCO back transitions.

REFERENCES

[1] GROEBNER, R.J., *et al.*, Phys. Rev. Lett. **64** (1990) 3015.

[2] BIGLARI, H., DIAMOND, P.H., TERRY, P.W., Phys. Fluids B **2** (1990) 1.

[3] BURRELL, K.H., Phys. Plasmas **4** (1997) 1499.

[4] BURRELL, K.H., *et al.*, Plasma Phys. Control. Fusion **46** (2004) 165.

[5] KOIDE, Y., *et al.*, Phys. Rev. Lett. **72** (1994) 3663.

[6] LEVINTON, F., *et al.*, Phys. Rev. Lett. **80** (1998) 4887.

[7] GREENFIELD, C.M., *et al.*, Phys. Rev. Lett. **86** (2001) 4544.

[8] SHAFER, M.W., *et al.*, Phys. Rev. Lett. **103** (2009) 075004.

[9] McKEE, G.R., *et al.*, Nucl. Fusion **49** (2009) 115016.

[10] ZWEBEN, S.J., *et al.*, Phys. Plasmas **17** (2010) 102502.

[11] CONWAY, G.D., *et al.*, Phys. Rev. Lett. **106** (2011) 065001.

[12] XU, G.S., *et al.*, Phys. Rev. Lett. **107** (2011) 125001.

[13] ESTRADA, T., *et al.*, Phys. Rev. Lett. **107** (2011) 245004.

[14] SCHMITZ, L., *et al.*, Phys. Rev. Lett. **108** (2012) 155002.

[15] KIM, E.J., and DIAMOND, P.H., Phys. Rev. Lett. **90** (2003) 185006.

[16] MIKI, K. et al, Phys. Plasmas **19** (2012) 092306.

[17] MANZ, P., *et al.*, Phys. Plasmas 19 (2012) 072311.

[18] TYNAN, G.R., *et al.*, this conference.

[19] AUSTIN, M., *et al.*, Phys. Plasmas **13** (2006) 082502.

[20] WALTZ, R.E, *et al.*, Phys. Plasmas **13** (2006) 052301.

[21] HILLESHEIM, J.C., *et al.*, Rev. Sci. Instrum. **80** (2009) 083507.

[22] PEEBLES, W.A., *et al.*, Rev. Sci. Instrum. **81** (2010) 10D902.

[23] HILLESHEIM, J.C., *et al.*, Rev. Sci. Instrum. **81** (2010) 10D907.

[24] DIAMOND, P.H., *et al.*, this conference.

ACKNOWLEDGMENT

This work was supported in part by the U.S. Department of Energy under DE-FG03-01ER54615, DE-FG02-08ER54984, DE-FC02-04ER54698, DE-FG02-89ER53296, DE-FG02-08ER54999, DE-AC02-09CH11466 and DE-FG02-07ER54917.